On the reliability of analytical models to predict solute transport in a fracture network

Claudia Cherubini*, Concetta I. Giasi**, Nicola Pastore**

*HydrISE, Institut Polytechnique LaSalle Beauvais, 19 rue Pierre Waguet, 60026 Beauvais Cedex, France

** Polytechnical University of Bari, Bari, Italy

Abstract

In hydrogeology, the application of reliable tracer transport model approaches is a key issue to derive the hydrodynamic properties of aquifers.

Laboratory and field – scale tracer dispersion breakthrough curves (BTC) in fractured media are notorious for exhibiting early time arrivals and late – time tailing that are not captured by the classical advection – dispersion equation (ADE). These ‘‘non – Fickian’’ features are proved to be better explained by a mobile – immobile (MIM) approach. In this conceptualization the fractured rock system is schematized as a continuous medium in which the liquid phase is separated into flowing and stagnant regions.

The present study compares the performances and reliabilities of the classical Mobile – Immobile Model (MIM) and the Explicit Network Model (ENM) that takes expressly into account the network geometry for describing tracer transport behaviour in a fractured sample at bench scale. Though ENM shows better fitting results than MIM, the latter remains still valid as it proves to describe the observed curves quite well.

The results show that the presence of nonlinear flow plays an important role in the behaviour of solute transport. Firstly the distribution of solute according to different pathways is not constant but it is related to the flow rate. Secondly nonlinear flow influences advection, in that it leads to a delay in solute transport respect to the linear flow assumption. Whereas nonlinear flow does not show to be related with dispersion. The experimental results show that in the study case the geometrical dispersion dominates the Taylor dispersion. However the interpretation with the ENM model shows a weak transitional regime from geometrical dispersion to Taylor dispersion for high flow rates. Incorporating the description of the flowpaths in the analytical modeling has proved to better fit the curves and to give a more robust interpretation of the solute transport.

Introduction

In fractured rock formations, the rock mass hydraulic behaviour is controlled by fractures. In such aquifers, open and well – connected fractures constitute high permeability pathways and are orders of magnitude more permeable than the rock matrix (Bear & Berkowitz, 1987; Berkowitz, 2002; Bodin et al., 2003; Cherubini, 2008; Cherubini & Pastore, 2011, Geiger et al., 2012, Neuman, 2005).

In most studies examining hydrodynamic processes in fractured media, it is assumed that flow is described by Darcy's law, which expresses a linear relationship between pressure gradient and flow rate (Cherubini & Pastore, 2010). Darcy's law has been demonstrated to be valid at low flow regimes ($Re < 1$). For $Re > 1$ a nonlinear flow behaviour is likely to occur.

But in real rock fractures, microscopic inertial phenomena can cause an extra macroscopic hydraulic loss (Kløv, 2000) which deviates flow from the linear relationship among pressure drop and flow rate.

To experimentally investigate fluid flow regimes through deformable rock fractures, Zhang & Nemcik (2013) carried out flow tests through both mated and non – mated sandstone fractures in triaxial cell. For water flow through mated fractures, the experimental data confirmed the validity of linear Darcy's law at low velocity. For larger water flow through non – mated fractures, the relationship between pressure gradient and volumetric flow rate revealed that the Forchheimer equation offers a good description for this particular flow process. The obtained experimental data show that Izbash's law can also provide an excellent description for nonlinear flow. They concluded that further work was needed to study the dependency of the two coefficients on flow velocity.

In fracture networks heterogeneity intervenes even in solute transport: due to the variable aperture and heterogeneities of the fracture surfaces the fluid flow will seek out preferential paths (Gylling et al., 1995) through which solutes are transported.

Generally the geometry of fracture network is not well known and the study of solute transport behaviour is based on multiple domain theory according to which the fractured medium is separated in two distinct domains: high velocity zones such as the network of connected fractures (mobile domain) where solute transport occurs predominantly by advection, and lower velocity zones such as secondary pathways, stagnation zones (almost – immobile domain), such as the rock matrix.

The presence of steep concentration gradients between fractures and matrix causes local disequilibrium in solute concentration which gives rise to dominantly diffusive exchange between

fracture and matrix. This explains the non – Fickian nature of transport, which is characterized by breakthrough curves with early first arrival and long tails.

Quantifying solute transport in fractured media has become a very challenging research topic in hydrogeology over the last three decades (Nowamooz et al., 2013, Cherubini et al., 2009).

Tracer tests are commonly conducted in such aquifers to estimate transport parameters such as effective porosity and dispersivity, to characterize subsurface heterogeneity, and to directly delineate flow paths. Transport parameters are estimated by fitting appropriate tracer transport models to the breakthrough data.

In this context, analytical models are frequently employed, especially for analyzing tests obtained under controlled conditions, because they involve a small number of parameters and provide physical insights into solute transport processes (Liu et al 2012).

The advection – dispersion equation (ADE) has been traditionally applied to model tracer transport in fractures. However extensive evidence has shown that there exist two main features that cannot be explained by the ADE: the early first arrival and the long tail of the observed BTCs curves. (Neretnieks et al, 1982; Becker and Shapiro, 2000; Jiménez-Hornero et al. 2005; Bauget and Fourar, 2008).

Several other models have been used to fit the anomalous BTCs obtained in laboratory tracer tests carried out in single fractures. Among those, the Mobile-Immobile (MIM) model (van Genuchten and Wierenga, 1976), has showed to provide better fits of BTC curves (Gao et al., 2009, Schumer et.al 2003, Feehley et al, 2010).

In the well – controlled laboratory tracer tests carried out by Qian et al. (2011) a mobile– immobile (MIM) model proved to fit both peak and tails of the observed BTCs better than the classical ADE model.

Another powerful method to describe non – Fickian transport in fractured media is the continuous time random walk (CTRW) approach (Berkowitz et al. 2006) which is based on the conceptual picture of tracer particles undergoing a series of transitions of length s and time *t*.

Together with a master equation conserving solute mass, the random walk is developed into a transport equation in partial differential equation form. The CTRW has been successfully applied for describing non – Fickian transport in single fractures (Berkowitz et al.2001; Jiménez – Hornero et al. 2005).

Bauget and Fourar (2008) investigated non – Fickian transport in a transparent replica of a real single fracture. They employed three different models including ADE, CTRW, and a stratified model to interpret the tracer experiments.

As expected, the solution derived from the ADE equation appears to be unable to model long-time tailing behaviour. On the other hand, the CTRW and the stratified model were able to describe non – Fickian dispersion. The parameters defined by these models are correlated to the heterogeneities of the fracture.

Nowamooz et al., (2013) carried out experimental investigation and modeling analysis of tracer transport in transparent replicas of two Vosges sandstone natural fractures.

The obtained breakthrough curves were then interpreted using a stratified medium model that incorporates a single parameter permeability distribution to account for fracture heterogeneity, together with a CTRW model, as well as the classical ADE model.

The results confirmed poorly fitting breakthrough curves for ADE. In contrast, the stratified model provides generally satisfactory matches to the data (even though it cannot explain the long-time tailing adequately) while the CTRW model captures the full evolution of the long tailing displayed by the breakthrough curves.

Qian et al (2011) experimentally studied solute transport in a single fracture (SF) under non – Darcian flow condition which was found to closely follow the Forchheimer equation.

They also investigated on the influence of the velocity contrast between the fracture wall and the plane of symmetry on the dispersion process, which was called ‘boundary layer dispersion’ by Koch and Brady (1985). They affirmed that this phenomenon had to be considered if the thickness of the boundary layer was greater than the roughness of the fracture. On the other hand, if the thickness of the boundary layer was smaller than the roughness of the fractures, the recirculation zones inside the roughness cavities rather than the boundary layer would be more relevant for the dispersion process, thus the hold – up dispersion would become important. Since smooth parallel planes were used for constructing the SF in their experiment, the fracture roughness and the hold – up dispersion were negligible.

Bodin et al (2007) developed the SOLFRAC program, which performs fast simulations of solute transport in complex 2D fracture networks using the Time Domain Random Walk (TDRW) approach (Delay & Bodin, 2001) that makes use of a pipe network approximation. The code accounts for advection and hydrodynamic dispersion in channels, matrix diffusion, diffusion into stagnant zones within the fracture planes, mass sharing at fracture intersections, and other mechanisms such as sorption reactions and radioactive decay. Comparisons between numerical results and analytical breakthrough curves for synthetic test problems have proven the accuracy of the model.

Zafarani & Detwiler (2013) presented an alternate approach for efficiently simulating transport through fracture intersections. Rather than solving the two – dimensional Stokes equations, the

model relies upon a simplified velocity distribution within the fracture intersection, assuming local parabolic velocity profiles within fractures entering and exiting the fracture intersection. Therefore, the solution of the two – dimensional Stokes equations is unnecessary, which greatly reduces the computational complexity. The use of a time – domain approach to route particles through the fracture intersection in a single step further reduces the number of required computations. The model accurately reproduces mixing ratios predicted by high – resolution benchmark simulations.

As most of previous investigations of flow and transport in fracture networks considered Darcian flow, the behaviour of the solute transport in fracture networks under non – darcian flow conditions has been therefore poorly investigated. In fracture networks different pathways can be identified through which solute is generally distributed in function of the energy spent by solute particles to cross the path. In this context the presence of nonlinear flow could play an important role in the distribution of the solutes according to the different pathways. In fact the energy spent to cross the path should be proportional to the resistance to flow associated to the single pathway, which in nonlinear flow regime is not constant but depends on the flow rate. This means that changing the boundary conditions the resistance to flow varies and as a consequence the distribution of solute in the main and secondary pathways also changes giving rise to a different behaviour of solute transport.

In previous studies by Cherubini et al (2012, 2013) the presence of nonlinear flow and non fickian transport in a fractured rock formation has been analyzed at bench scale in laboratory tests. The effects of nonlinearity in flow have been investigated by analyzing hydraulic tests on an artificially created fractured limestone block of parallelepiped ($0.60\times0.40\times0.8$ m^3) shape.

The flow tests regard the observation of the volumes of water passing through different paths across the fractured sample. In particular, the inlet flow rate and the hydraulic head difference between the inlet and outlet ports have been measured. The experimental results have shown evidence of a non-Darcy relationship between flow rate and hydraulic head differences that is best described by a polynomial expression. Transition from viscous dominant regime to inertial dominant regime has been detected. The experiments have been compared with a 3d numerical model in order to evaluate the linear and non-linear terms of Forchheimer equation for each path.

Moreover, a tortuosity factor has been determined which is a measure of the deviation of each flow path from the parallel plate model. A power law has been detected between the Forchheimer terms and the tortuosity factor, which means that the latter influences flow dynamics.

The non fickian nature of transport has been investigated by means of tracer tests that regard the measurement of breakthrough curves for saline tracer pulse across a selected path varying the flow rate. The observed experimental breakthrough curves of solute transport have proved to be better

modeled by the 1d analytical solution of MIM model. The carried out experiments show that there exists a pronounced mobile–immobile zone interaction that cannot be neglected and that leads to a non-equilibrium behaviour of solute transport. The existence of a non-Darcian flow regime has showed to influence the velocity field in that it gives rise to a delay in solute migration with respect to the predicted value assuming linear flow. Furthermore the presence of inertial effects has proved to enhance non-equilibrium behaviour. Instead, the presence of a transitional flow regime seems not to exert influence on the behaviour of dispersion.

Herein, in order to give a more physical interpretation of the flow and transport behaviour, we build on the work by Cherubini et al (2013) by interpreting the obtained experimental results of flow and transport tests by means of the comparison of two conceptual models: the 1d single rate mobile – immobile model (MIM) and the 2d Explicit Network Model (ENM). Differently from the former, the latter expressly takes the fracture network geometry into account.

When applied to fractured media, the MIM approach does not explicitly take the fracture network geometry into account, but it conceptualizes the shape of fractures as 1d continuous media in which the liquid phase is separated into flowing and stagnant regions. The convective dispersive transport is restricted to the flowing region, and the solute exchange is described as a first – order process.

Unlike MIM, the ENM model may allow to know the physical meaning of flow and transport phenomena (i.e the meaning of long – time behaviour of BTC curves that characterize fractured media) and permits to obtain a more accurate estimation of flow and solute transport parameters. In this model the fractures are represented as 1d – pipe elements and they form a 2d – pipe network.

It is clear that ENM needs to address the problem of parameterization. In fact the transport parameters of each individual fracture should be specified and this leads to more uncertainty in the estimation.

Our overarching objective is therefore of investigating the performances and the reliabilities of MIM and ENM approaches to describe conservative tracer transport in a fractured rock sample.

In particular way the present paper focuses the attention on the effects of nonlinear flow regime on different features that depict the conservative solute transport in a fracture network such as mean travel time, dispersion, dual porosity behaviour, distribution of solute into different pathways.

Theoretical background

Nonlinear flow

In the literature different laws are reported that account for the nonlinear relationship between velocity and pressure gradient.

A cubic extension of Darcy's law that describes pressure loss versus flow rate for low flow rates is the weak inertia equation:

$$-\frac{dp}{dx} = \frac{\mu}{k} \cdot v + \frac{\gamma \rho^2}{\mu} \cdot v^3 \quad (1)$$

Where p ($ML^{-1}T^{-2}$) is the pressure, k (L^2) is the permeability, μ ($ML^{-1}T^{-1}$) is the viscosity, ρ (ML^{-3}) is the density, v (LT^{-1}) is the velocity and γ(L) is called the weak inertia factor.

In case of higher Reynolds numbers (Re >> 1) the pressure losses pass from a weak inertial to a strong inertial regime, described by the Forchheimer equation (Forchheimer, 1901), given by:

$$-\frac{dp}{dx} = \frac{\mu}{k} \cdot v + \rho \beta \cdot v^2 \quad (2)$$

Where β (L^{-1}) is called the inertial resistance coefficient, or non – Darcy coefficient.

Forchheimer law can be written in terms of hydraulic head:

$$-\frac{dh}{dx} = a' \cdot v + b' \cdot v^2 \quad (3)$$

Where a' (TL^{-1}) and b' (TL^{-2}) are the linear and inertial coefficient respectively equal to:

$$a' = \frac{\mu}{\rho g k};\ b' = \frac{\beta}{g} \quad (4)$$

In the same way the relationship between flow rate Q (L^3T^{-1}) and hydraulic head gradient can be written as:

$$-\frac{dh}{dx} = a \cdot Q + b \cdot Q^2 \quad (5)$$

Where a (TL^{-3}) and b (T^2L^{-6}) are related to a' and b':

$$a = \frac{a'}{\omega_{eq}};\ b = \frac{b'}{\omega_{eq}} \quad (6)$$

Where ω_{eq} (L^2) represents the equivalent cross sectional area of fracture.

Mobile Immobile Model

The mathematical formulation of the MIM for non - reactive solute transport is usually given as follows:

$$\frac{\partial c_m}{\partial t} = D\frac{\partial^2 c_m}{\partial x^2} - v\frac{\partial c_m}{\partial x} - \alpha\left(c_m - c_{im}\right)$$
$$\beta\frac{\partial c_{im}}{\partial t} = \alpha\left(c_m - c_{im}\right) \quad (7)$$

Where t (T) is the time, x (L) is the spatial coordinate along the direction of the flow, c_m and c_{im} (ML^{-3}) are the cross - sectional averaged solute concentrations respectively in the mobile and immobile domain, v (LT^{-1}) is the average flow velocity and D (L^2T^{-1}) is the dispersion coefficient, α (T^{-1}) is the mass exchange coefficient, β [-] is the mobile water fraction. For a non – reactive solute β is equivalent to the ratio between the immobile and mobile cross – sectional area (-).

The solution of system Equation (7) describing one – dimensional (1d) non – reactive solute transport in an infinite domain for instantaneous pulse of solute injected at time zero at the origin is given by (Goltz & Roberts, 1986):

$$c_m(x,t) = e^{-\alpha t}c_0\left(x,t\right) + \alpha\int_0^t H\left(t,\tau\right)c_0\left(x,\tau\right)d\tau \quad (8)$$

Where c_0 represents the analytical solution for the classical advection – dispersion equation (Crank, 1956):

$$c_0(x,t) = \frac{M_0}{\omega_{eq}\sqrt{\pi D t}}e^{-\frac{(x-vt)^2}{4Dt}} \quad (9)$$

Where Mo (M) is the mass of the tracer injected instantaneously at time zero at the origin of the domain. The term $H\left(t,\tau\right)$ presents the following expression:

$$H\left(t,\tau\right) = e^{-\frac{\alpha}{\beta}(t-\tau)-\alpha\tau}\frac{\tau I_1\left(\frac{2\alpha}{\beta}\sqrt{\beta(t-\tau)\tau}\right)}{\sqrt{\beta(t-\tau)\tau}} \quad (10)$$

Where I_1 represents the modified Bessel function of order 1.

In order to fit the BTCs curves with the MIM model the assumption of representative 1d length (L) of the fracture network should be made. However this matter can be solved by the introduction of the normalized velocity (v/L) and normalized dispersion (D/L^2). The MIM model is defined by four parameters regarding the whole fracture network (v/L, D/L^2, α, β).

Explicit Network Model

Assuming that a single fracture *j* can be represented by a 1d – pipe element, the relationship between head loss Δh_j (L) and flow rate Q_j (L^3T^{-1}) can be written in finite terms on the basis of Forchheimer model:

$$\frac{\Delta h_j}{l_j} = aQ_j + bQ_j^2 \Rightarrow \Delta h_j = \left[l_j \left(a + bQ_j \right) \right] Q_j \tag{11}$$

Where l_j (L) is the length of fracture, a (TL^{-3}) and b (T^2L^{-6}) are the Forchheimer parameters in finite terms.

The term in the square brackets represents the resistance to flow $R_j\left(Q_j\right)$ (TL^{-3}) of *j* fracture.

For steady – state condition and for a 2d simple geometry of the fracture network, the solution of flow field can be obtained in a straightforward manner applying the first and second Kirchhoff's laws.

The first law affirms that the algebraic sum of flow in a network meeting at a point is zero:

$$\sum_{j=1}^{n} Q_j = 0 \tag{12}$$

Whereas the second law affirms that the algebraic sum of the head losses along a closed loop of the network is equal to zero:

$$\sum_{j=1}^{n} \Delta h_j = 0 \tag{13}$$

Generally in a 2d fracture network, the single fracture can be set in series and/or in parallel.

In particular the total resistance to flow of a network in which the fractures are arranged in a chain is found by simply adding up the resistance values of the individual fractures.

In a parallel network the flow breaks up by flowing through each parallel branch and re – combining when the branches meet again. The total resistance to flow is found by adding up the reciprocals of the resistance values and then taking the reciprocal of the total. The flow rate crossing the generic fracture *j* belonging to parallel circuits Q_j can be obtained as:

$$Q_j = \sum Q \frac{1}{R_j} \left(\sum_{i=1}^{n} \frac{1}{R_i} \right)^{-1} \quad (14)$$

Where $\sum Q$ (LT^{-3}) is the sum of the discharge flow evaluated for the fracture intersection located in correspondence of the inlet bond of *j* fracture, whereas the term in brackets represents the probability of water distribution of *j* fracture $P_{Q,j}$.

The BTC curves at the outlet of the network $c_{out}(t)$ (ML^{-3}), for an instantaneous injection, can be obtained as the summation of BTCs of each elementary path in the network. The latter can be expressed as the convolution product of the probability density functions of residence times in each individual fracture belonging to the elementary path. Using the convolution theorem, $c_{out}(t)$ can be expressed as:

$$c_{out}(t) = \frac{M_0}{Q_0} F^{-1} \left[\sum_{i=1}^{N_{ep}} \prod_{j=1}^{n_{f,i}} P_{c,j} F\left(s_j\left(l_j, t \right) \right) \right] \quad (15)$$

Where M_0 (M) is the injected mass of solute, *F* is the Fourier transform operator, N_{ep} is the number of elementary paths, $n_{f,i}$ is the number of fractures in *i* elementary path, $P_{c,j}$ and $s_j\left(l_j, t\right)$ (T^{-1}) represent the fraction of solute crossing the single fracture and the probability density function of residence time respectively.

$P_{c,j}$ can be estimated as the probability of the particle transition in correspondence of the inlet bond of each individual single fracture. The rules for particle transition through fracture intersections play an important role in mass transport. In literature several models have been developed and tested in order to represent the mass transfer within fracture intersections. The simplest rule is represented by the “perfect mixing model” in which the mass sharing is proportional to the relative discharge flow rates.

The perfect mixing model assumes that the probability of particle transition of the fraction of solute crossing the single fracture can be written as:

$$P_{c,j} = \frac{Q_j}{\sum Q} \quad (16)$$

Where Q_j represents the flow rate in the single *j* fracture. Note that if assuming valid the perfect mixing model $P_{Q,j}$ is equal to $P_{c,j}$.

285 It is clear that in order to know $s_j\left(l_j,t\right)$ the transport model and consequently the transport
286 parameters of each single fracture need to be defined. $s_j\left(l_j,t\right)$ can be evaluated in a simple way
287 using the 1D analytical solution of the Advection Dispersion Equation model (ADE) for pulse
288 input:

289 $$s_j(l_j,t)=\frac{Q_j}{\omega_{eq,j}\sqrt{\pi D_j t}}e^{-\frac{\left(l_j-v_j t\right)^2}{4D_j t}} \tag{17}$$

290 in which the velocity v_j and dispersion D_j relating to the generic j fracture can be estimated through
291 the following expression:

292 $$v_j=\frac{Q_j}{\omega_{eq,j}} \tag{18}$$

293 $$D_j=\alpha_{L,j}v_j \tag{19}$$

294 Where $\omega_{eq,j}$ and $\alpha_{L,j}$ are the equivalent crossing area and the dispersion coefficient of j fracture
295 respectively.

296 The ENM is defined by six parameters regarding each single fracture (a, b , P_Q, ω_{eq}, α_L and P_c).

297 # Material and methods

298 **Flow and tracer tests**

299 The experimental setup has been already extensively discussed in Cherubini et al. (2013), however
300 for the completeness in this section a summary is reported. The analysis of flow dynamics through
301 the selected path (Fig 2) regards the observation of water flow from the upstream tank to the flow
302 cell with a circular cross-section of 0.1963 m^2 and 1.28×10^{-4} m^2 respectively.

303 Initially at time t_0, the valves '*a*' and '*b*' are closed and the hydrostatic head in the flow cell is equal
304 to h_0. The experiment begins with the opening of the valve '*a*' which is reclosed when the hydraulic
305 head in the flow cell is equal to h_1. Finally the hydraulic head in the flow cell is reported to h_0
306 through the opening of the valve '*b*'. The experiment procedure is repeated changing the hydraulic
307 head of the upstream tank h_c. The time $\Delta t=\left(t_1-t_0\right)$ required to fill the flow cell from h_0 to h_1 has
308 been registered.

Given that the capacity of the upstream tank is much higher than that of the flow cell it is reasonable to assume that during the experiments the level of the upstream tank (h_c) remains constant. Under this hypothesis the flow inside the system is governed by the equation:

$$S_1 \frac{dh}{dt} = \Gamma(\Delta h)(h_c - h) \tag{20}$$

Where S_1 (L^2) and h (L) are respectively the section area and the hydraulic head of the flow cell; h_c (L) is the hydraulic head of upstream tank, $\Gamma(\Delta h)$ represents the hydraulic conductance term representative of both hydraulic circuit and the selected path.

The average flow rate $\bar{Q}$ can be estimated by means of the volumetric method:

$$\bar{Q} = \frac{S_1}{t_1 - t_0}(h_1 - h_0) \tag{21}$$

Whereas the average hydraulic head difference $\overline{\Delta h}$ is given by:

$$\overline{\Delta h} = h_c - \frac{h_0 + h_1}{2} \tag{22}$$

In correspondence of the average flow rate and head difference is it possible to evaluate the average hydraulic conductance as:

$$\bar{\Gamma}(\Delta h) = \frac{S_1}{t_1 - t_0} \ln\left(\frac{h_0 - h_c}{h_1 - h_c}\right) \tag{23}$$

The inverse of $\bar{\Gamma}(\Delta h)$ represents the average resistance to flow $\bar{R}(\bar{Q})$.

The study of solute transport dynamics through the selected path has been carried out by means of a tracer test using sodium chloride. Initially a hydraulic head difference between the upstream tank and downstream tank is imposed. At t = 0 the valve '*a*' is closed and the hydrostatic head inside the block is equal to the downstream tank. At t = 10 s the valve '*a*' is opened while at time t = 60 s a mass of solute equal to 5×10^{-4} kg is injected into the inlet port through a syringe. The source release time (1 s) is very small therefore the instantaneous source assumption can be considered valid.

In correspondence of the flow cell in which the multi - parametric probe is located it is possible to measure the tracer breakthrough curve and the hydraulic head; in the meanwhile the flow rate

entering the system is measured by means of an ultrasonic velocimeter. For different flow rates a BTC curve can be recorded at the outlet port.

Time moment analysis has been applied in order to characterize the BTC curves in terms of mean breakthrough time, degree of spread and asymmetry.

The mean residence time t_m is given by:

$$t_m = \frac{\int_0^\infty t^n c(t)dt}{\int_0^\infty c(t)dt} \tag{24}$$

The n[th] normalized central moment of distribution of solute concentration versus time is defined as:

$$\mu_n = \frac{\int_0^\infty [t - t_m]^n c(t)dt}{\int_0^\infty c(t)dt} \tag{25}$$

The second moment μ_2 represents the degree of spread relative to t_m whereas the degree of asymmetry measured by the skewness coefficient is defined as:

$$S = \mu_3 / \mu_2^{3/2} \tag{26}$$

Discussion

Estimation of flow model parameters

The flow field in each single fracture of the network can be solved in analytical way by means of Kirchhoff laws. In Figure 2 is represented the 2d – pipe network conceptualization.

The resistance to flow of each single *j* fracture is described by the Equation (12). The Forchheimer parameters are assumed constant for the whole fracture network.

The application of the Kirchhoff's first law at the node 3 can be written as:

$$Q_0 - Q_1 - Q_2 = 0 \tag{27}$$

Whereas the application of the Kirchhoff's second law at the loop 3 – 4 – 5 – 6 can be written as:

$$R_6(Q_1)Q_1 - \left(R_3(Q_2) + R_4(Q_2) + R_5(Q_2)\right)Q_2 = 0 \tag{28}$$

Substituting Equation (27) into Equation (28) the iterative equation of flow rate Q_1 can be obtained:

$$Q_1^{k+1} = Q_0 \left[\frac{R_3\left(Q_0 - Q_1^k\right) + R_4\left(Q_0 - Q_1^k\right) + R_5\left(Q_0 - Q_1^k\right)}{R_3\left(Q_0 - Q_1^k\right) + R_4\left(Q_0 - Q_1^k\right) + R_5\left(Q_0 - Q_1^k\right) + R_6\left(Q_1^k\right)} \right] \tag{29}$$

The Forchheimer parameters representative of whole fracture network can be derived matching the average resistance to flow derived experimentally with the resistance to flow evaluated for the whole network:

$$\bar{R}\left(\bar{Q}\right) = R_1\left(Q_0\right) + R_2\left(Q_0\right) + \left(\frac{1}{R_6\left(Q_1\right)} + \frac{1}{R_3\left(Q_2\right) + R_4\left(Q_2\right) + R_5\left(Q_2\right)} \right)^{-1} + \\ + R_7\left(Q_0\right) + R_8\left(Q_0\right) + R_9\left(Q_0\right) \tag{30}$$

Figure 3 shows the fitting of observed resistance to flow determined by the inverse of Equation (23) and the theoretical resistance to flow (Equation 30). The linear and nonlinear terms of Forchheimer model in Equation (12) have been estimated and they are respectively equal to $a = 7.345\times10^4$ sm^{-3} and $b = 11.65\times10^9$ s^{2}m^{-6}. It is evident that the 2d - pipe network model closely matches the experimental results ($r^2 = 0.9913$). Flow characteristics can be studied through the analysis of Forchheimer number F_0 which represents the ratio of nonlinear to linear hydraulic gradient contribution:

$$F_o = \frac{bQ}{a} \tag{31}$$

Inertial forces dominate over viscous ones at the critical Forchheimer number (F_o=1) corresponding in our case to a flow rate equal to $Q_{crit} = 6.30\times10^{-6}$ m^3/s, which is coherent with the results obtained in the previous study (Cherubini et al., 2013a).

The term in square brackets in Equation (30) represents the probability of water distribution P_Q evaluated for the branch 6. Note that it is not constant but it depends on the flow rate crossing the parallel branch. Figure 4 shows P_Q as function of Q_0. The probability of water distribution decreases as the injection flow rate increases. This means that when the injection flow rate increases the resistance to flow of the branch 6 increases faster than the resistance to flow of the branch 3 – 4 – 5 and therefore the solute choses the secondary pathway.

Fitting of breakthrough curves and interpretation of estimated transport model parameters

Several tests have been conducted in order to observe solute transport behaviour varying the injection flow rate in the range 1.20×10^{-6} - 9.34×10^{-6} m^3s^{-1}. For each experimental BTCs the mean travel time t_m and the coefficient of Skewness S have been estimated.

Figure 5 shows t_m as function of Q_0. Travel time decreases more slowly for high flow rates. In particular a change of slope is evident in correspondence of the injection flow rate equal to 4×10^{-6} m^3s^{-1} (Cherubini et al., 2013a), which means the setting up of a transitional flow regime; the diagram of velocity profile is flattened because of inertial forces prevailing on viscous one, as already showed by Cherubini et al (2013a). The presence of a transitional flow regime leads to a delay on solute transport with respect to the values that can be obtained under the assumption of a linear flow field. Note that this behaviour occurs before Q_{crit}.

The skewness coefficient does not exhibit a trend upon varying the injection flow rate, but its mean value is equal to 2.018. A positive value of skewness indicates that BTCs are asymmetric with early first arrival and long tail. This behaviour seems not to be dependent on the presence of the transitional regime.

The measured breakthrough curves for different flow rates have been individually fitted by MIM $\left(v/L,\ D/L^2,\ \alpha,\ \beta\right)$ and ENM $\left(\omega_{eq},\ \alpha_L,\ P_Q,\ P_C\right)$ models.

In particular for the ENM model the parameters ω_{eq} (equivalent area) and α_L are representative of all fracture network, whereas the parameters P_Q and P_C are associated only to the parallel branches. For the considered fracture network the Equation (15) becomes:

$$c_{out} = \frac{M_0}{Q_0} F^{-1}\left[\begin{array}{l} P_c \cdot F(s_1)\cdot F(s_2)\cdot F(s_6)\cdot F(s_7)\cdot F(s_8)\cdot F(s_9) + \\ +(1-P_c)\cdot F(s_1)\cdot F(s_2)\cdot F(s_3)\cdot F(s_4)\cdot F(s_5)\cdot F(s_7)\cdot F(s_8)\cdot F(s_9)\end{array}\right] \quad (32)$$

The velocity and dispersion that characterize the probability density function s are related to the flow rate that crosses each branch by Equations (18) and (19). This one is equal to the injection flow rate Q_0 except for branch 6 and branches 3 – 4 – 5 for which it is equal to $Q = P_Q Q_0$ and $Q = \left(1-P_Q\right)Q_0$ respectively.

Furthermore three parameter configurations have been tested for the ENM model. The configurations are distinguished on the basis of the number of fitting parameters and assumptions

made on P_C and P_Q parameters. The first configuration named ENM2 has two fitting parameters ω_{eq} and α_L. In this configuration P_C is imposed equal to P_Q and is derived as the square brackets term in Equation (29).

The second configuration named ENM3 has three fitting parameters ω_{eq}, α_L and P_C (P_Q). P_C is still equal to P_Q but they are evaluated by the interpretation of BTC curves.

In the third configuration named ENM4 all four parameters $\left(\omega_{eq},\ \alpha_L,\ P_Q,\ P_C\right)$ are determined through the fitting of BTCs.

To compare all the considered models, both the determination coefficient (r^2) and the root mean square error (RMSE) were used as criteria to determine the goodness of the fitting, which can be expressed as:

$$r^2 = 1 - \frac{\sum_{i=1}^{N}\left(C_{i,o} - C_{i,e}\right)^2}{\sum_{i=1}^{N}\left(C_{i,o} - \bar{C}_{i,o}\right)^2} \tag{33}$$

$$RMSE = \sqrt{\frac{1}{N}\sum_{i=1}^{N}\left(C_{i,o} - C_{i,e}\right)^2} \tag{34}$$

Where N is the number of observations, $C_{i,e}$ is the estimated concentration, $C_{i,o}$ is the observed concentration and $\bar{C}_{i,o}$ represents the mean value of $C_{i,o}$.

Tables 1, 2, 3 and 4 show the estimated values of parameters, root mean square error RMSE and the determination coefficient r^2 for all the considered models varying the inlet flow rate Q_0.

Figure 6 shows the fitting results of BTC curves for different injection flow rates.

For higher flow rates (7.07×10^{-6} and 4.80×10^{-6} m^3/s) the fitting is poorer than for lower flow rates (3.21×10^{-6} and 1.96×10^{-6} m^3/s). However, all models provide a satisfactory fitting. The ENM4 model provides the highest values of r^2 varying in the range 0.9921 – 1.000 and the smallest values of RMSE in the range 0.0033 – 0.0252. This is expected for two reasons. First this model has more fitting parameters than ENM2 and ENM3, thus it is more flexible. Second, compared to MIM model, it takes explicitly into account the presence of the secondary path.

The MIM model considers the existence of immobile and mobile domains and a rate – limited mass transfer between these two domains. In the present context this conceptualization can be a weak assumption especially for high flow rates when the importance of secondary path increases. However the fitting of BTCs shows that MIM model remains valid as it proves to describe the observed curves quite well.

The extent of solute mixing can be assessed from the analysis of MIM first-order mass transfer coefficient α and the fraction of mobile water β.

Several authors have observed the variation of the mass-transfer coefficient between mobile and immobile water regions with pore-water velocity (van Genuchten and Wierenga, 1977; Nkedi-Kizza et al., 1984; De Smedt and Wierenga, 1984; De Smedt et al., 1986; Schulin et al., 1987). The increase in α with increasing water velocity is attributed to higher mixing in the mobile phase at high pore water velocities (De Smedt and Wierenga, 1984) or to shorter diffusion path lengths as a result of a decrease in the amount of immobile water (van Genuchten and Wierenga, 1977).

As concerns β, various authors have observed different behaviour of the mobile water fraction parameter. Gaudet et al. (1977) reported increasing mobile water content with increasing pore water velocity. However, studies have also found that β appears to be constant with varying pore-water velocity (Nkedi-kizza et al. 1983). However, lower β values can be attributed to faster initial movement of the solute as it travels through a decreasing number of faster flow paths. As a result, some authors have related β values to the initial arrival of the solute. In fact, Gaudet et al. (1977) and Selim and Ma (1995) observed that the mobile water fraction parameter affects the time of initial appearance of the solute.

In general, the initial breakthrough time increases as β increases (Gao et al., 2009) which can also be evidenced from Fig 6. For lower flow rates the initial arrival time is higher than for higher flow rates. As the fraction of mobile water increases, the breakthrough curves are shifted to longer times because the solute is being transported through larger and larger fractions of the fracture volume. In the limiting case that the fraction of mobile water reaches one, the MIM reduces to the equilibrium ADE (no immobile water) (Mulla & Strock, 2008).

The evidence of dual porosity behaviour on solute transport is clearly shown by the analysis of the two MIM parameters: the ratio of mobile and immobile area β and the mass exchange coefficient α, shown in Figure 7 as a function of velocity.

A different behaviour of these two coefficients to varying the injection flow rate is observed in the present study. At Darcian-like flow conditions the mass exchange coefficient remains constant,

459 whereas the ratio of mobile and immobile area decreases as velocity increases. When nonlinear
460 flow starts to become dominant a different behaviour is observed: α increases in a potential way,
461 whereas β assumes a weakly growing trend as velocity increases with a mean value equal to 0.56.

462 In order to better explain this behaviour, the transport time (reciprocal of normalized velocity) and
463 the exchange time (reciprocal of the exchange term) varying the flow rate for the MIM model are
464 showed in Figure 8. In analogous way in Figure 9 is showed the comparison between the mean
465 travel time for the main path and the secondary path varying the injection flow rate for the ENM4
466 model.

467 For the MIM model at high flow rates the exchange time joins the transport time; analogously for
468 the ENM4 as the flow rate increases the secondary path reaches the main path in terms of mean
469 travel time. This analogy between MIM and ENM enhances the concept that the mass transfer
470 coefficient is dependent on flow velocity.

471 In Darcian-like flow conditions the main path is dominant on the secondary path. The latter can be
472 considered as an immobile zone. In this condition the fracture network behaves as a single fracture
473 and the observed dual porosity behaviour can be attributable only to the fracture – matrix
474 interactions of the main path.

475 For higher velocities, a higher contact area between the mobile and immobile region is evidenced,
476 enhancing solute mixing between these two regions (Gao et al, 2009). The increase in α with
477 increasing water velocity is therefore attributable to nonlinear flow that enhances the exchange
478 between the main and secondary flow paths. Increasing the injection flow rate the importance of the
479 secondary path grows and the latter cannot be considered as an immobile zone, as a consequence
480 the dual porosity behaviour becomes stronger.

481 As showed in figure 10 and 11 P_Q as function of Q_0 evaluated by means the fitting of BTCs by
482 ENM3 and ENM4 models presents a different trend respect to P_Q determined by means of flow
483 tests. P_Q evaluated by transport tests decreases more rapidly than P_Q determined by flow tests
484 (Figure 10). In the ENM4 model P_Q and P_C show a different behaviour, especially for higher
485 velocity P_C presents values higher than P_Q (Figure 11). In other words the interpretation of BTC
486 curves evidences more enhanced nonlinear flow behaviour than the flow tests.

487 In Figure 12 is reported the relationship between velocity v and injection flow rate Q_0 . Note that, in
488 order to compare the results, the velocities for MIM are evaluated assuming the length of the

medium equal to the length of main path (L = 0.601 m). Instead for ENM4 model the velocities are evaluated dividing Q_0 for the equivalent area ω_{eq}. The models present the same behaviour, and similarly to the mean travel time a change of slope is evident again in correspondence of flow rate equal to 4×10^{-6} m^3s^{-1}. This result confirms the fact that the presence of nonlinear flow regime leads to a delay on solute transport with respect to the values that can be obtained under the assumption of a linear flow field.

In order to better represent the nonlinear flow regime, Figure 13 shows water pressure as a function of velocity. A change of slope is evident for $v = 1.5\times10^{-2}$ ms^{-1} which corresponds to the flow rate equal to 4×10^{-6} m^3s^{-1}.

Moreover as shown in Figure 14 a linear trend of dispersion with the injection flow rate both for MIM and ENM models has been observed. This is coherent with what obtained in the previous study (Cherubini et al. 2013a) where a linear relationship is found between velocity and dispersion both for ADE and MIM models with the conclusion that geometrical dispersion dominated the effects of Aris – Taylor dispersion. The values of the coefficient of dispersion obtained for ENM models do not depend on flow velocity but assume a somehow scattered but fluctuating value. Being α_L values constant, geometrical dispersion dominates the mixing processes along the fracture network. Therefore, the presence of a nonlinear flow regime does not prove to exert any influence on dispersion except for high velocities for the ENM model where a weak transitional regime appears.

This does not happen for MIM dispersion values whose rates of increase are smaller than those of ENM dispersion values.

The values of dispersion coefficient are in order of magnitude of decimeter, which is comparable with the values obtained for darcian condition (Qian et al, 2011), and the dispersion values of MIM are much lower than those of ENM.

This may be attributable to the fact that the MIM separates solute spreading into dispersion in mobile region and mobile-immobile mass transfer. The dispersive effect is therefore partially taken into account by the mass transfer between the mobile zone and the immobile zone (Qian et al, 2011; Gao et al, 2009).

Conclusion

Flow and tracer test experiments have been carried out in a fracture network. The aim of the present study is that of comparing the performances and reliabilities of two model paradigms: the Mobile -

Immobile Model (MIM) and the Explicit Network Model (ENM) to describe conservative tracer transport in a fractured rock sample.

Fluid flow experiments show a not negligible nonlinear behaviour of flow best described by the Forchheimer law. The solution of the flow field for each single fracture highlights that the probabilities of water distribution between the main and the secondary path are not constant but decrease as the injection flow rate increases. In other words varying the injection flow rate the conductance of the main path decreases more rapidly than the conductance of the secondary path.

The BTCs curves determined by transport experiments have been fitted by MIM model and three versions of ENM model (ENM2, ENM3, ENM4) which differ on the basis of the assumptions made on the parameters P_Q and P_C. All models show a satisfactory fitting. The ENM4 model provides the best fit which is expectable because it has more fitting parameters than ENM2 and ENM3, thus it is more flexible. Secondly, compared to MIM model, it takes explicitly into account the presence of the secondary path. Furthermore for the ENM model the parameter P_Q decreases more rapidly varying the injection flow rate than the same parameter determined by flow tests. The relationship between transport time and exchange time for MIM model and mean travel time for main path and secondary path for the ENM4 model varying the injection flow rate has shown similarity of behaviour: for higher values of flow rate the difference between transport time and exchange time decreases and the secondary path reaches the main path in terms of mean travel time. This analogy between MIM and ENM explains the fact that the mass transfer coefficient is dependent on flow velocity. The mass transfer coefficient increases as the importance of secondary path over the main path increases.

The velocity values evaluated for MIM and ENM model show the same relationship with the injection flow rate. In particular a change of slope is evident in correspondence of the flow rate equal to 4×10^{-6} m^3s^{-1}. This behaviour occurs before the critical flow rate estimated by flow tests equal to 6.3×10^{-6} m^3s^{-1}. Therefore the interpretation of BTCs curves evidences more enhanced nonlinear behaviour than flow tests. These results confirm the fact that the presence of transitional flow regime leads to a delay on solute transport with respect to the values that can be obtained under the assumption of a linear flow field (Cherubini et al., 2013a).

As concerns dispersion, a linear trend varying the velocity for both MIM and ENM models has been observed -coherently with the previous results- (Cherubini et al., 2013a), the MIM model underestimating the dispersion respect to ENM4 model.

551 The dispersivity values obtained for ENM models do not depend on flow velocity but assume a
552 somehow scattered but fluctuating value. Being α_L values constant, geometrical dispersion
553 dominates the mixing processes along the fracture network. Therefore, the presence of a nonlinear
554 flow regime does not prove to exert any influence on dispersion except for high velocities for the
555 ENM model where a weak transitional regime seems to appear. This result demonstrates that for our
556 experiment geometrical dispersion still dominates Taylor dispersion.

557 A major challenge for tracer tests modeling in fractured media is the adequate choice of the
558 modeling approach for each different study scale.

559 When dealing with large scales, tracer tests breakthrough curves are generally modeled by a
560 relatively small number of model parameters (Becker and Shapiro, 2000).

561 At laboratory scale, the definition of the network of fractures by means of discrete approaches
562 (DFN) can permit to identify transport pathways and mass transport coefficients, in order to better
563 define heterogeneous advective phenomena (Cherubini et. al, 2013b).

564 At an intermediate local field scale (1-100m), recognition that heterogeneous environments contain
565 fast and slow paths led to the development of the MIM formulation applied successfully in a variety
566 of hydrogeologic settings. However, the assumed velocity partitioning into flowing and not-flowing
567 zones is not an accurate representation of the true velocity field (Gao et al., 2009). Especially when
568 the rock mass is sparsely fractured, the breakthrough curves are characterized by early breakthrough
569 and long tailing behaviour and a simple mobile-immobile conceptualization may be an over
570 simplification of the physical transport phenomenon.

571 Solute transport in fractured aquifers characterized by highly non-Fickian behaviour is therefore
572 better described by an Explicit Network Model rather than by a simple MIM. Applying a discrete
573 model in such a case can permit to determine if transport occurs through one or several fractures
574 and if multiple arrivals are caused by fracture heterogeneity, in such a way as to yield a more robust
575 interpretation of the subsurface transport regime.

576 In such a context, geophysical imaging may provide detailed information about subsurface structure
577 and dynamics (Dorn et al, 2012).

578 **References**

579 Bauget, F. and Fourar, M.: Non-Fickian dispersion in a single fracture, J. Contam. Hydrol., 100,
580 137–148, doi:10.1016/j.jconhyd.2008.06.005, 2008.

581 Bear, J.: Dynamics of Fluids in Porous Media, Elsevier, New York, 1972.

582 Bear, J. and Berkowitz, B.: Groundwater flow and pollution in fractured rock aquifers, in:
583 Developments in Hydraulic Engineering, vol. 4, edited by: Novak, P., Elsevier Applied Science
584 Publishers Ltd., New York, 175–238, 1987.

585 Becker, M. W. and Shapiro, A. M.: Tracer transport in fractured crystalline rock: evidence of
586 nondiffusive breakthrough tailing, Water Resour. Res., 36, 1677–1686,
587 doi:10.1029/2000WR900080, 2000.

588 Berkowitz, B.: Characterizing flow and transport in fractured geological media: a review, Adv.
589 Water Resour., 25, 861–884, 2002.

590 Berkowitz, B., Cortis, A., Dentz, M., and Scher, H.: Modeling non-Fickian transport in geological
591 formations as a continuous time random walk, Rev. Geophys., 44, RG2003,
592 doi:10.1029/2005RG000178, 2006.

593 Bodin, J., Delay, F., and de Marsily, G.: Solute transport in a single fracture with negligible matrix
594 permeability: 1. fundamental mechanisms, Hydrogeol. J., 11, 418–433, 2003.

595 Bodin, J., Porel, G., Delay, F., Ubertosi, F., Bernard, S., and de Dreuzy, J.: Simulation and analysis
596 of solute transport in 2-D fracture/pipe networks: the SOLFRAC program, J. Contam. Hydrol., 89,
597 1–28, 2007.

598 Cherubini, C.: A modeling approach for the study of contamination in a fractured aquifer, in:
599 Geotechnical and Geological Engineering, vol. 26, Springer, the Netherlands, 519–533, 2008.

600 Cherubini, C. and Pastore, N.: Modeling contaminant propagation in a fractured and karstic aquifer,
601 Fresen. Environ. Bull., 19, 1788–1794, 2010.

602 Cherubini, C. and Pastore, N.: Critical stress scenarios for a coastal aquifer in southeastern Italy,
603 Nat. Hazards Earth Syst. Sci., 11, 1381–1393, doi:10.5194/nhess-11-1381-2011, 2011.

604 Cherubini, C., Giasi, C.I., Pastore, N.: Application of Modelling for Optimal Localisation of
605 Environmental Monitoring Sensors, Proceedings of the Advances in sensor and Interfaces (IWASI),
606 Trani, Italy, 2009, 222-227, 2009

607 Cherubini, C., Giasi, C. I., and Pastore, N.: Bench scale laboratory tests to analyze non-linear flow
608 in fractured media, Hydrol. Earth Syst. Sci., 16, 2511–2522, doi:10.5194/hess-16-2511-2012, 2012.

609 Cherubini, C., Giasi, C. I., and Pastore, N.: Evidence of non-Darcy flow and non-Fickian transport
610 in fractured media at laboratory scale, Hydrol. Earth Syst. Sci., 17, 2599–2611, doi:10.5194/hess-
611 17-2599-2013, 2013a.

612 Cherubini, C., Giasi, C. I., and Pastore, N.: Fluid flow modeling of a coastal fractured karstic
613 aquifer by means of a lumped parameter approach, Environ. Earth Sci., 70, 2055–2060, 2013b.

614 Delay, F. and Bodin, J.: Time domain random walk method to simulate transport by advection–
615 dispersion and matrix diffusion in fracture networks, Geophys. Res. Lett., 28, 4051–4054, 2001.

616 De Smedt, F. and Wierenga, P. J.: Solute transfer through columns of glass beads, Water Resour.
617 Res., 20, 225–232, 1984.

618 Feehley, C. E., Zheng, C., and Molz, F. J.: A dual-domain mass transfer approach for modeling
619 solute transport in heterogeneous aquifers: Application to the Macrodispersion Experiment
620 (MADE) site, Water Resour. Res., 36, 2501–2515, 2010.

621 Forchheimer, P.: Wasserbewegung durch Boden, Z. Verein Deut. Ing., 45, 1781–1788, 1901.

622 Gaudet, J. P., Jégat, H., Vachaud, G., and Wierenga, P. J.: Solute transfer, with exchange between
623 mobile and stagnant water, through unsaturated sand, Soil Sci. Soc. Am. J., 41,665–671, 1977.

624 Geiger, S., Cortis, A., and Birkholzer, J. T.: Upscaling solute transport in naturally fractured porous
625 media with the continuous time random walk method, Water Resour. Res., 46,
626 doi:10.1029/2010WR009133, 2010.

627 Gylling, B., Moreno, L., and Neretnieks, I.: Transport of solute in fractured media, based on a
628 channel network model, in: Proceedings of Groundwater Quality: Remediation and Protection
629 Conference, edited by: Kovar, K. and Krasny, J., 14–19 May, Prague, 107–113, 1995.

630 Jiménez-Hornero, F. J., Giráldez, J. V., Laguna, A., and Pachepsky, Y.: Continuous time
631 randomwalks for analyzing the transport of a passive tracer in a single fissure, Water Resour. Res.,
632 41, W04009, doi:10.1029/2004WR003852, 2005.

633 Kamra, S. K., Lennartz, B., van Genuchten, M. T., andWidmoser, P.: Evaluating non-equilibrium
634 solute transport in small soil columns, J. Contam. Hydrol., 48, 189–212, 2001.

635 Klov, T.: High-velocity flow in fractures, Dissertation for the partial fulfillment of the requirements
636 for the degree of doktor ingenieur Norvegian University of Science Technology Department of
637 Petroleum Engineering and Applied Geophysics, Trondheim, 2000.

638 Liu, H. H., Mukhopadhyay, S., Spycher, N., and Kennedy, B. M.: Analytical solutions of tracer
639 transport in fractured rock associated with precipitation-dissolution reactions, Hydrogeol. J.,19,
640 1151–1160, 2011.

641 Moutsopoulos, K. N., Papaspyros, I. N. E., and Tsihrintzis, V. A.: Experimental investigation of
642 inertial flow processes in porous media, J. Hydrol., 374, 242–254, 2009.

643 Mulla, D. J. and Strock, J. S.: Nitrogen transport processes in soil, in: Nitrogen in agricultural
644 systems, edited by: Schepers, J. S. and Raun,W. R., Agron. Monogr. 49, ASA, CSSA, SSSA,
645 Madison, WI, 401–436, 2008.

646 Neretnieks, I., Eriksen, T., and Tahtinen, P.: Tracer movement in a single fissure in granitic rock:
647 some experimental results and their interpretation, Water Resour. Res., 18, 849–858,
648 doi:10.1029/WR018i004p00849, 1982.

649

650

651

652

MIM 1

n°	Q (m^3/s)×10^{-6}	v/L(s^{-1})×10^{-2}	D/L^2 (s^{-1})×10^{-2}	α (s^{-1})×10^{-2}	β (-)	RMSE	r^2
1	1.319	0.73 ± 0.05	0.15 ± 0.01	0.43 ± 0.09	0.95 ± 0.14	0.022	0.979
5	2.209	1.05 ± 0.05	0.16 ± 0.01	0.50 ± 0.12	0.51 ± 0.07	0.021	0.991
10	2.731	1.26 ± 0.05	0.18 ± 0.01	0.60 ± 0.12	0.51 ± 0.06	0.021	0.994
15	3.084	1.74 ± 0.06	0.19 ± 0.01	1.03 ± 0.16	0.56 ± 0.05	0.023	0.995
20	3.365	1.75 ± 0.06	0.20 ± 0.01	1.06 ± 0.17	0.54 ± 0.05	0.022	0.996
25	3.681	2.49 ± 0.10	0.25 ± 0.02	1.67 ± 0.32	0.51 ± 0.06	0.030	0.995
30	4.074	2.57 ± 0.11	0.26 ± 0.02	1.67 ± 0.35	0.50 ± 0.06	0.033	0.994
35	4.536	2.25 ± 0.09	0.21 ± 0.02	1.58 ± 0.29	0.57 ± 0.06	0.031	0.994
40	5.382	3.20 ± 0.13	0.26 ± 0.02	2.68 ± 0.44	0.61 ± 0.06	0.035	0.994
45	5.895	3.32 ± 0.15	0.26 ± 0.02	2.82 ± 0.50	0.57 ± 0.06	0.036	0.995
50	6.168	3.02 ± 0.15	0.26 ± 0.02	2.52 ± 0.52	0.51 ± 0.07	0.031	0.996
55	8.345	3.54 ± 0.29	0.35 ± 0.04	3.05 ± 1.07	0.41 ± 0.11	0.038	0.995

654 Table 1. Estimated values of parameters, root mean square error RMSE and determination coefficient r^2 for mobile – immobile
655 model MIM at different injection flow rates in the fractured medium.

ENM 2

n°	Q (m^3/s)×10^{-6}	ω_{eq} (m^2)×10^{-4}	α_L (m)×10^{-1}	RMSE	R^2
1	1.3194	3.10 ± 0.14	1.92 ± 0.86	0.033	0.952
5	2.2090	3.22 ± 0.04	0.98 ± 0.06	0.020	0.993
10	2.7312	3.29 ± 0.04	0.92 ± 0.05	0.019	0.995
15	3.0842	2.81 ± 0.03	0.79 ± 0.03	0.020	0.996
20	3.3648	3.06 ± 0.03	0.79 ± 0.03	0.019	0.997
25	3.6813	2.35 ± 0.02	0.74 ± 0.03	0.026	0.996
30	4.0735	2.49 ± 0.02	0.75 ± 0.03	0.027	0.996
35	4.5356	3.27 ± 0.04	0.74 ± 0.04	0.028	0.995
40	5.3824	2.76 ± 0.02	0.75 ± 0.02	0.023	0.998
45	5.8945	2.90 ± 0.02	0.69 ± 0.02	0.027	0.997
50	6.1684	3.30 ± 0.04	0.68 ± 0.02	0.032	0.995
55	8.3455	3.56 ± 0.05	0.78 ± 0.02	0.041	0.994

657 **Table 2. Estimated values of parameters, root mean square error RMSE and determination coefficient r^2 for ENM2 at**
658 **different injection flow rates in the fractured medium.**

659

660

661

662

663

664

665

ENM 3

n°	Q (m^3/s)×10^{-6}	ω_{eq} (m^2)×10^{-4}	α_L (m)×10^{-1}	P_Q/P_C (-)	RMSE	R^2
1	1.319	3.43 ± 1.28	1.92 ± 0.86	0.82 ± 0.17	0.032	0.954
5	2.209	3.18 ± 0.11	0.98 ± 0.06	0.76 ± 0.02	0.020	0.993
10	2.731	3.28 ± 0.09	0.92 ± 0.05	0.75 ± 0.02	0.019	0.995
15	3.084	2.73 ± 0.05	0.79 ± 0.03	0.73 ± 0.01	0.019	0.997
20	3.365	2.94 ± 0.05	0.79 ± 0.03	0.72 ± 0.01	0.017	0.997
25	3.681	2.22 ± 0.04	0.74 ± 0.03	0.71 ± 0.01	0.023	0.997
30	4.074	2.37 ± 0.04	0.75 ± 0.03	0.71 ± 0.01	0.025	0.997
35	4.536	3.13 ± 0.06	0.74 ± 0.04	0.71 ± 0.01	0.026	0.995
40	5.382	2.61 ± 0.03	0.75 ± 0.02	0.70 ± 0.01	0.016	0.999
45	5.895	2.70 ± 0.03	0.69 ± 0.02	0.68 ± 0.01	0.016	0.999
50	6.168	2.98 ± 0.03	0.68 ± 0.02	0.66 ± 0.01	0.017	0.999
55	8.345	3.13 ± 0.02	0.78 ± 0.02	0.63 ± 0.01	0.016	0.999

Table 3. Estimated values of parameters, root mean square error RMSE and determination coefficient r^2 for ENM3 at different injection flow rates in the fractured medium.

ENM 4

n°	Q (m^3/s)×10^{-6}	ω_{eq} (m^2)×10^{-4}	α_L (m)×10-1	P_Q (-)	P_C (-)	RMSE	R^2
1	1.319	2.67 ± 0.13	1.18 ± 0.11	0.85 ± 0.02	0.67 ± 0.02	0.020	0.981
5	2.209	3.15 ± 0.12	0.96 ± 0.07	0.76 ± 0.02	0.75 ± 0.03	0.020	0.993
10	2.731	3.28 ± 0.10	0.92 ± 0.06	0.75 ± 0.02	0.76 ± 0.02	0.019	0.995
15	3.084	2.74 ± 0.06	0.80 ± 0.04	0.73 ± 0.01	0.74 ± 0.02	0.019	0.997
20	3.365	2.97 ± 0.06	0.81 ± 0.04	0.72 ± 0.01	0.73 ± 0.02	0.017	0.997
25	3.681	2.28 ± 0.05	0.80 ± 0.04	0.70 ± 0.01	0.74 ± 0.02	0.020	0.998
30	4.074	2.43 ± 0.06	0.80 ± 0.04	0.71 ± 0.01	0.74 ± 0.02	0.022	0.997
35	4.536	3.18 ± 0.08	0.76 ± 0.05	0.71 ± 0.01	0.73 ± 0.02	0.025	0.996
40	5.382	2.62 ± 0.04	0.76 ± 0.03	0.70 ± 0.01	0.70 ± 0.01	0.016	0.999
45	5.895	2.76 ± 0.03	0.73 ± 0.02	0.68 ± 0.01	0.71 ± 0.01	0.014	0.999
50	6.168	3.12 ± 0.04	0.76 ± 0.02	0.66 ± 0.01	0.71 ± 0.01	0.012	0.999
55	8.345	3.46 ± 0.02	0.96 ± 0.01	0.63 ± 0.00	0.73 ± 0.01	0.003	1.000

Table 4. Estimated values of parameters, root mean square error RMSE and determination coefficient r^2 for ENM4 at different injection flow rates in the fractured medium.

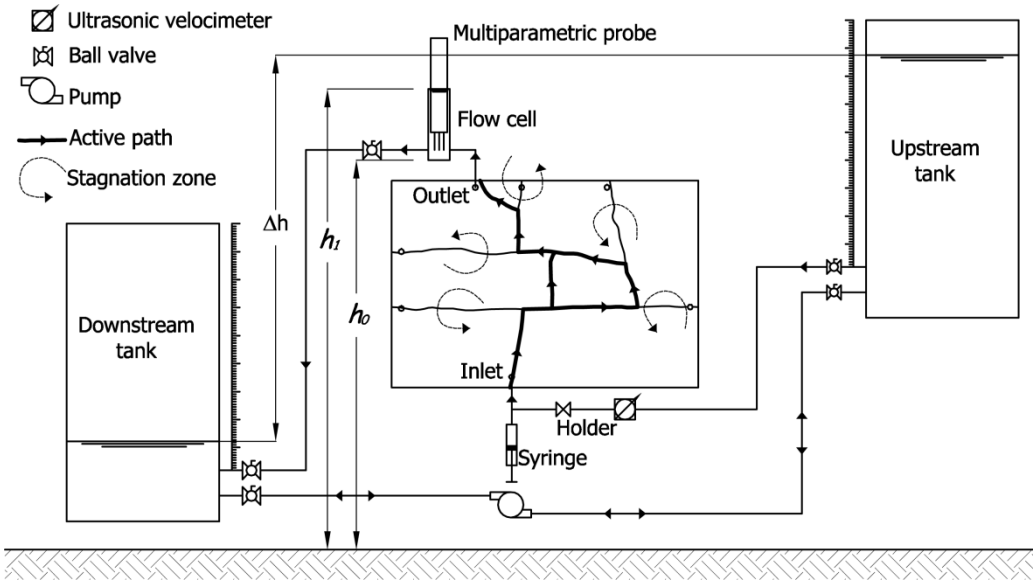

675

676 **Figure 1. Schematic diagram of experimental setup.**

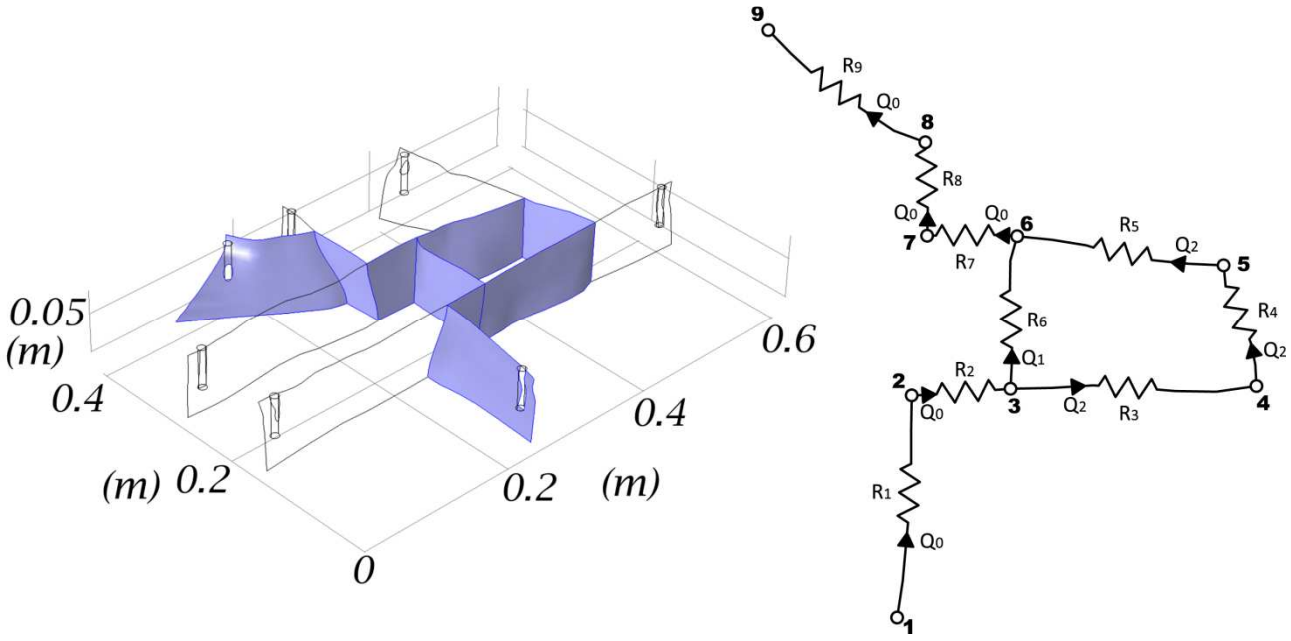

677

678 **Figure 2. 2d pipe network conceptualization of the fractured medium.**

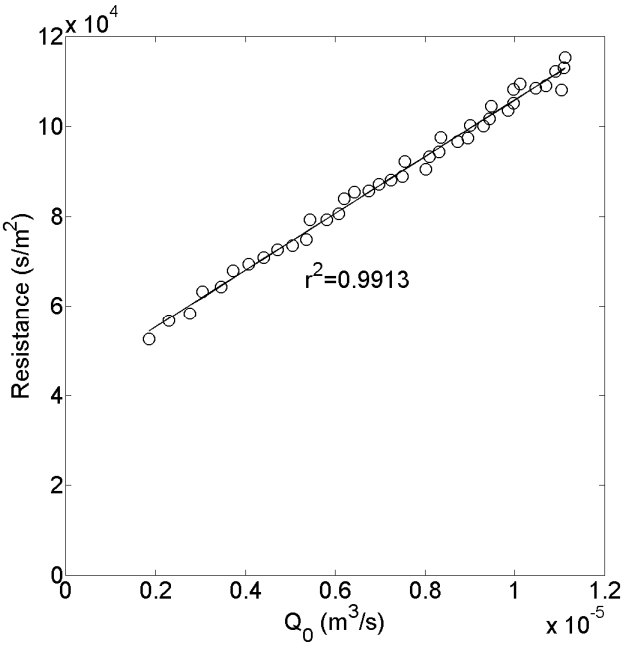

679

680 **Figure 3. Average resistance to flow versus injection flow rate Q_0 (m^3/s). The circles represent the experimental values, the**
681 **straight line represents the resistance to flow evaluated by equation (31).**

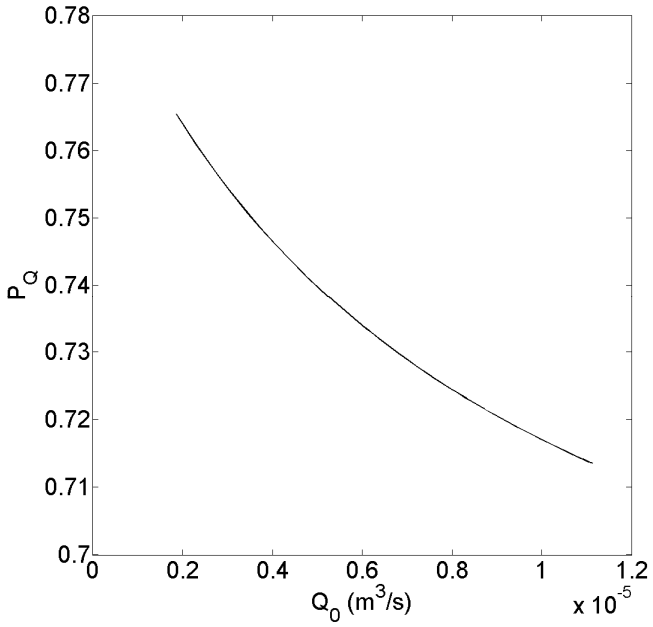

682

683 **Figure 4. Probability of water distribution evaluated for main path P_Q versus injection flow rate Q_0 (m^3/s).**

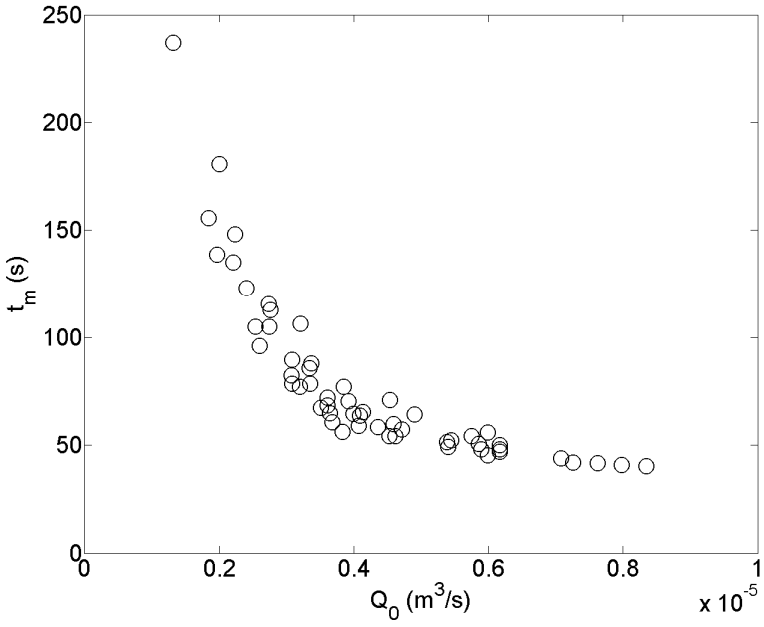

684

685 **Figure 5. Mean travel time t_m (s) versus injection flow rate Q_0 (m^3/s).**

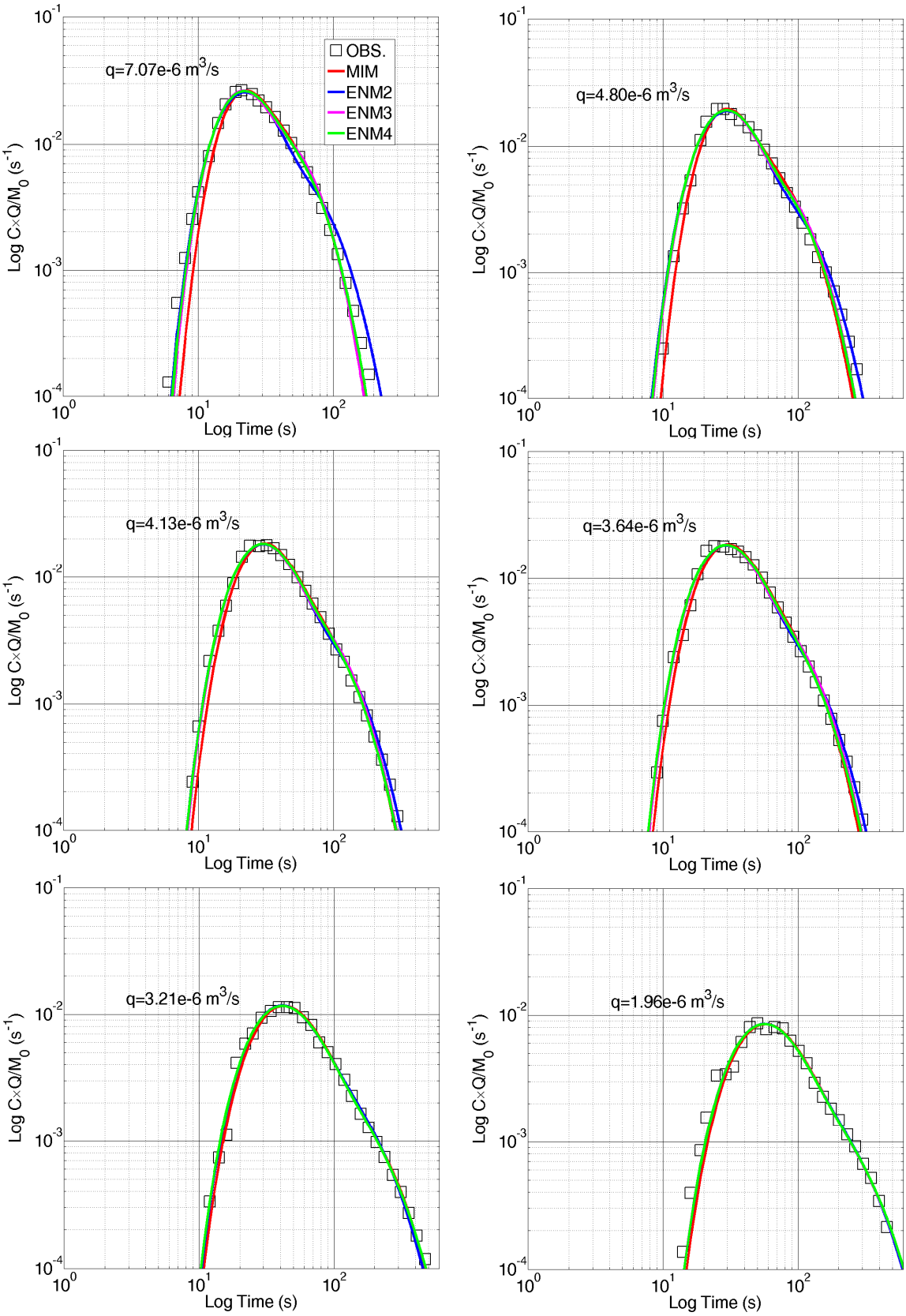

686

687 **Figure 6. Fitting of breakthrough curves at different injection flow rates using each of the four models (MIM, ENM1, ENM2,**
688 **ENM3).**

689

690

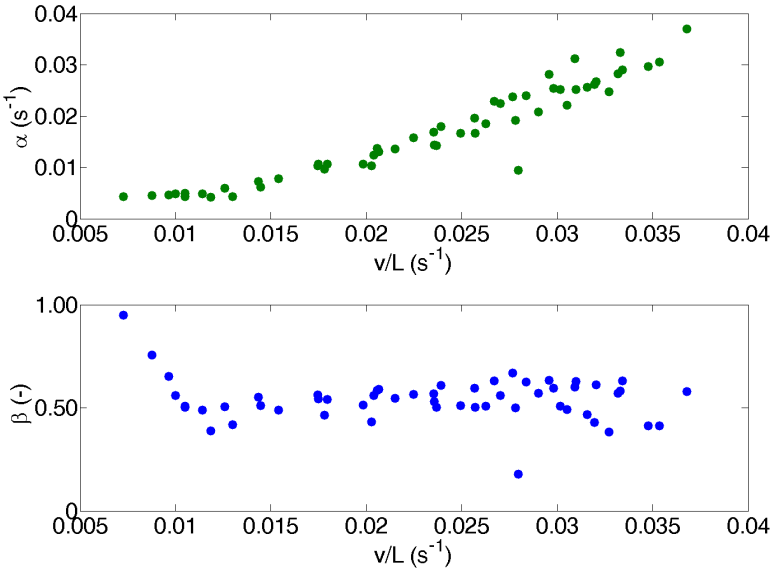

691

692 **Figure 7. Mass transfer coefficient α and fraction of mobile water β as function of normalized velocity v/L (s^{-1}) for MIM**
693 **model. An outlier is evidenced for v/L=0,028 s^{-1}**

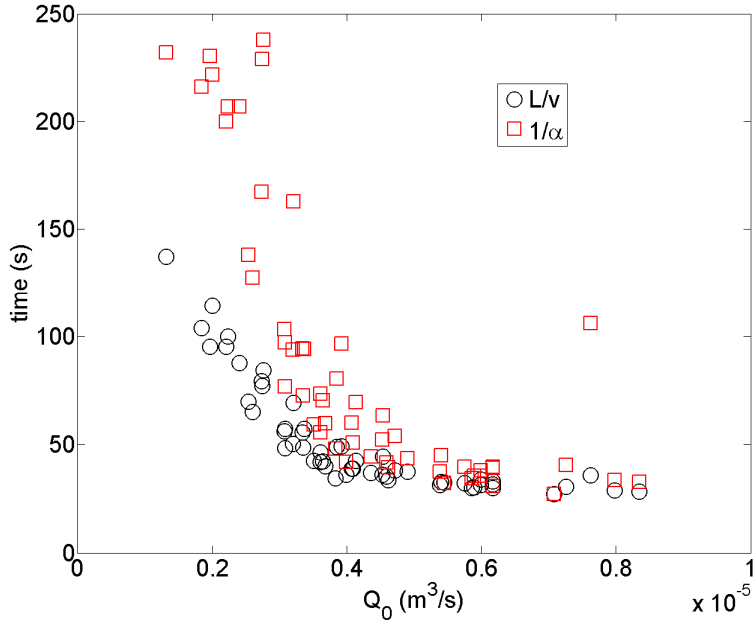

694

695 **Figure 8. Transport time (L/v) (reciprocal of normalized velocity) and exchange time (1/α) (reciprocal of the exchange term)**
696 **as function of injection flow rate Q_0 (m^3/s) for mobile - immobile model MIM.**

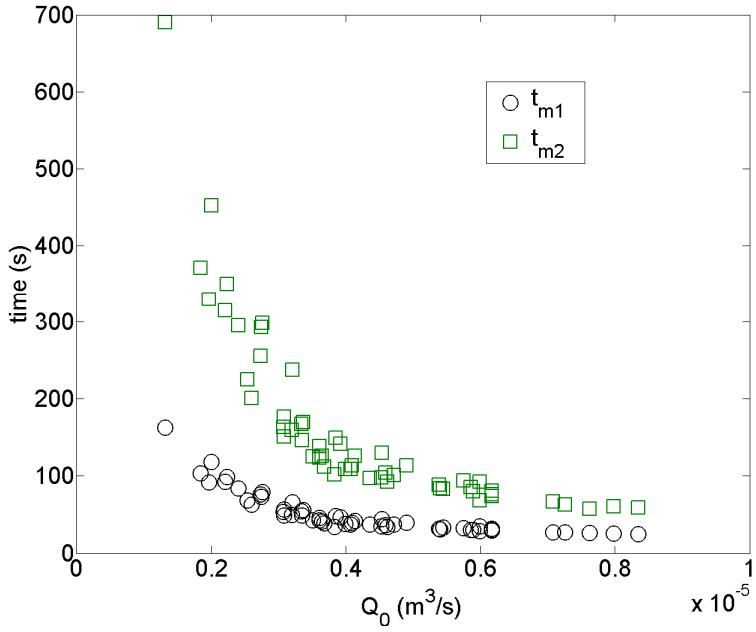

697

698 **Figure 9. Travel time for main path t_{m1} (s) and travel time for secondary path t_{m2} (s) for ENM4 as function of injection flow**
699 **rate Q_0 (m^3/s).**

700

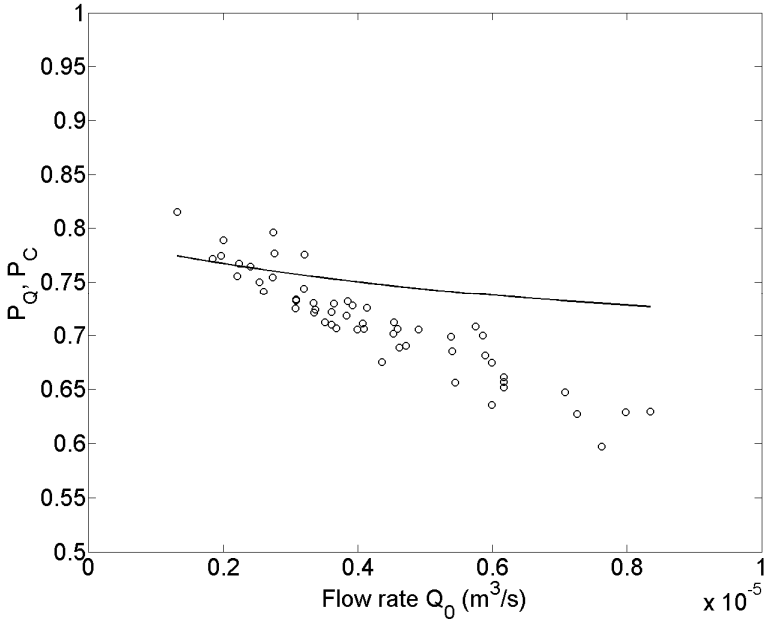

701

702 **Figure 10. Comparison between the Probability of water distribution P_Q evaluated as the square brackets term in Equation**
703 **(29) (straight line) and the probability of particle transition $P_C(P_Q)$ for ENM3 (circle) varying the injection flow rate Q_0**
704 **(m^3/s).**

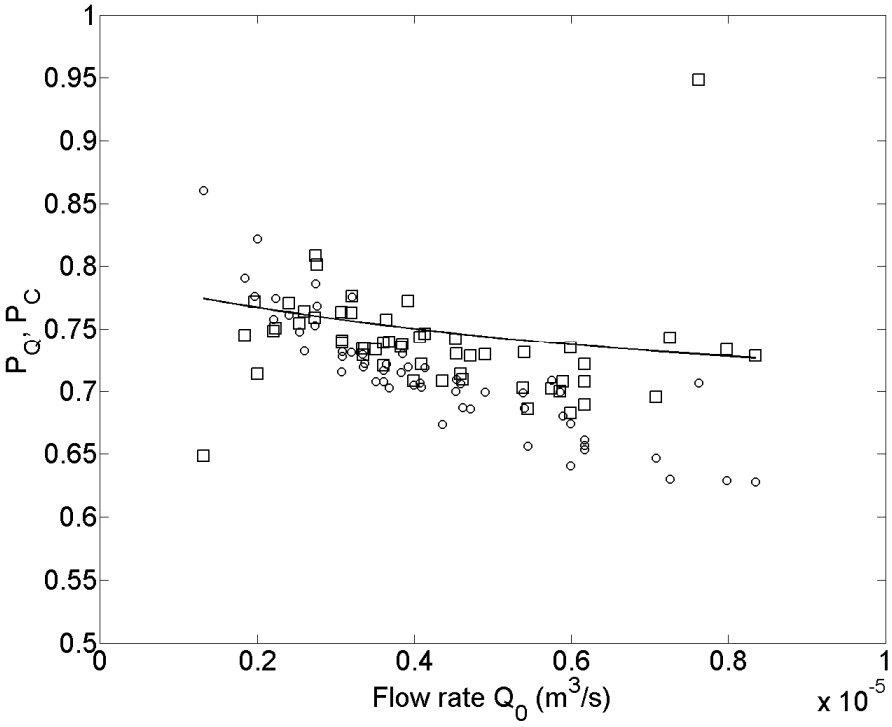

705

706 **Figure 11. Comparison between the Probability of water distribution P_Q evaluated by the flow model (straight line) and the**
707 **probability of particle transition P_c (square) and P_Q (circle) for ENM4 varying the injection flow rate Q_0 (m^3/s).**

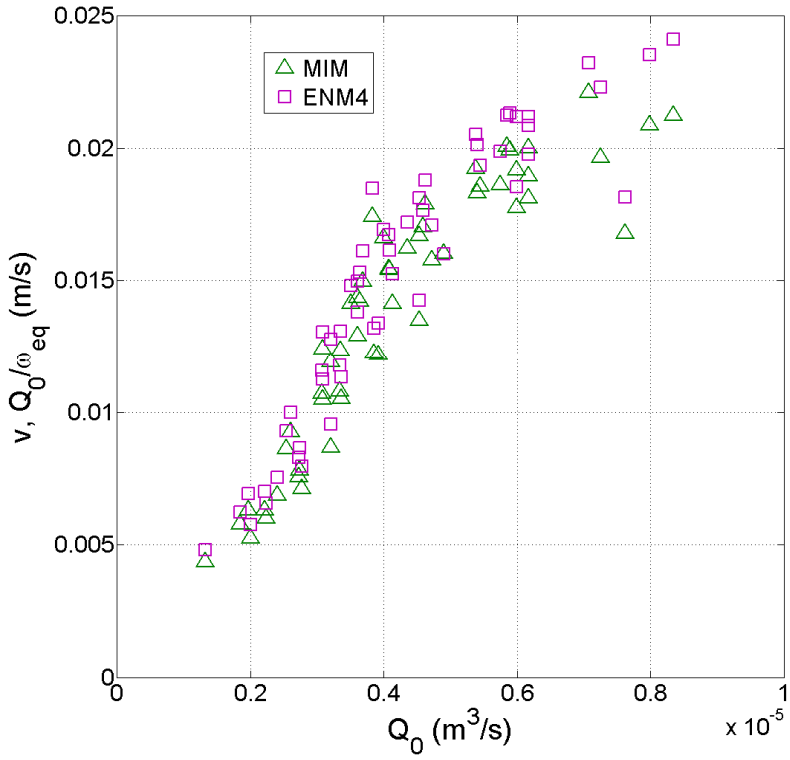

708

709 **Figure 12. velocity *v* (m/s) as function of the injection flow rate Q_0 (m^3/s) for MIM and ENM4 models. Note that for MIM**
710 **model the *v* is determined assuming the length of medium equal to the length of main path (*L* = 0.601 m). Instead for the**
711 **ENM4 model the velocity is determined dividing Q_0 for the equivalent area ω_{eq}.**

712

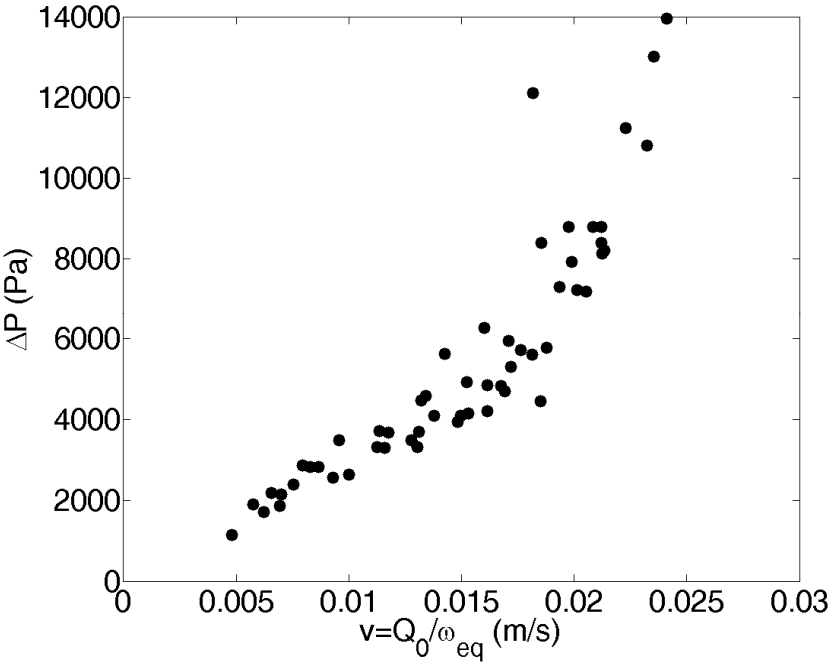

713

714 **Figure 13. difference of pressure ΔP (Pa) as function of velocity v (m/s) for ENM4. The velocity is determined dividing Q_0 for**
715 **the equivalent area ω_{eq}.**

716

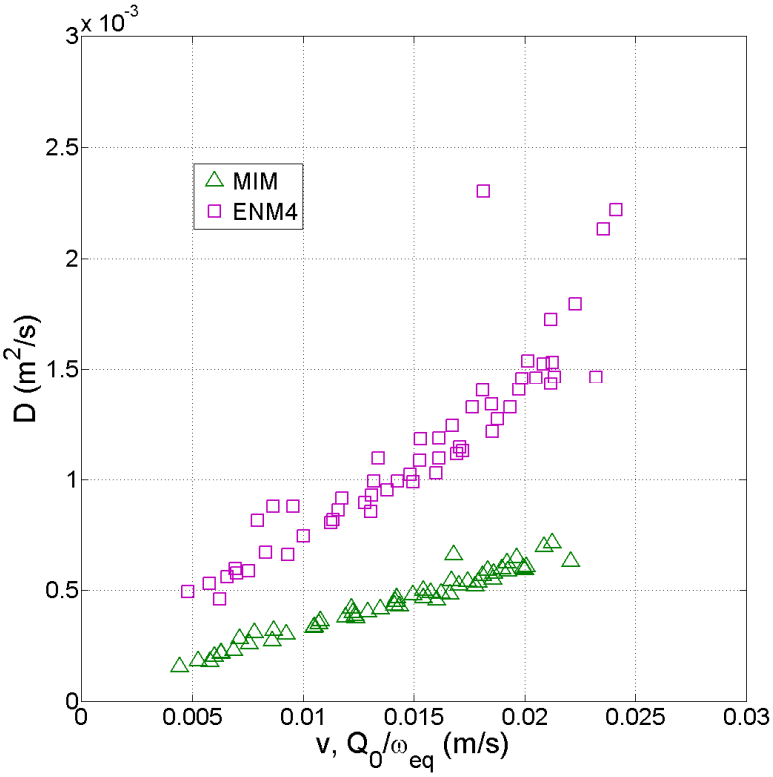

717

718 **Figure 14. Dispersion D (m^2/s) as function of velocity for MIM and ENM4 models. Note that for MIM model *D* is determined**
719 **assuming the length of the medium equal to the length of the main path (l=0.601 m). Instead for ENM4 model D is**
720 **determined as $D=Q_0 \cdot \alpha_L/\omega_{eq}$.**